Journal of Materiomics 7 (2021) 264–270

Contents lists available at ScienceDirect

Journal of Materiomics

journal homepage: www.journals.elsevier.com/journal-of-materiomics/

Tuning electroluminescence performance in Pr-doped piezoelectric bulk ceramics and composites

Hailing Sun [a, b, *], Manchung Wong [b], Guofu Zhou [a], K.W. Kwok [b, **]

[a] Guangdong Provincial Key Laboratory of Optical Information Materials and Technology & Institute of Electronic Paper Displays, South China Academy of Advanced Optoelectronics, South China Normal University, Guangzhou, 510006, China
[b] Department of Applied Physics, The Hong Kong Polytechnic University, Kowloon, China

ARTICLE INFO

Article history:
Received 10 July 2020
Received in revised form
7 October 2020
Accepted 21 October 2020
Available online 26 October 2020

Keywords:
Electroluminescence
Emission color tuning
Ferroelectric.
Piezoelectric
Doping

ABSTRACT

Alternating current electroluminescence (ACEL) shows great potential in lighting, display and intelligent skin. Herein, the ACEL properties of Pr^{3+}-doped $Ba_{0.85}Ca_{0.15}Ti_{0.90}Zr_{0.10}O_3$ ceramic and its PDMS-based composite have been investigated. Intense red EL emission was obtained in the ceramic sample whereas blue EL emission of Pr^{3+} was observed for the first time in the composite counterpart. The red EL emission should be attributed to the impact of hot electrons driven by the large piezoelectric electric field. Owing to the cross-relaxations through the 4f5d levels and Pr-to-metal charge transfer state, the ^3P_J emissions were completely quenched, and thus leading to an enhancement in red emission. However, external E field induced a large local piezoelectric deformation of the ceramic particles embedded in the PDMS matrix, which in turn caused a bending of CB and then a downwards shift of the 4f5d levels from the CB. Hence the cross-relaxations were hindered, and the blue EL emission was observed in the composites. The results would attract attention of functional materials studies and expand our understanding of such facile structure and oxide EL devices to facilitate their use in integral part of flexible device systems.

1. Introduction

Alternating current electroluminescence (ACEL) in metal-ion doped sulfide-based materials have been extensively studied for illumination, display and intelligent skin applications [1–4]. Since Inoguchi et al. introduced a double-insulating ZnS:Mn thin-film EL device in 1974, various sulfide-based EL materials and devices have been developed [5]. Different from ZnS:Mn which exhibited yellow-orange emission, Barrow et al. have revealed strontium sulfide doped with cerium (SrS:Ce) could emit blue-green light under electric field [6]. After that, SrS:Ce/ZnS:Mn multilayer structure exhibiting bright and stable white light has then been developed for use in color EL displays by Soininen et al. [7]. Apart from these thin-film phosphors, composite phosphors consisting of phosphors particles embedded in a polymeric matrix have also been widely studied for practical use. Stauffer et al. have fabricated a composite film comprising a large amount of $BaTiO_3$ and ZnS:Cu EL particles in a matrix of PDMS, which showed a significant luminance enhancement, reaching a high value of 121 cd/m^2 under a voltage of 250 V and 2.2 kHz [8]. It is generally known that free electrons and holes could been generated under a high electric field in phosphor layers [9]. For thin-film phosphors, the electrons are accelerated by the high electric field (usually in the order of 10^6 V/cm) to ballistic energies for impact-ionizing the luminescent centers and thereby leading to photon emission. On the other hand, as the applied electric field used for composite phosphors is generally lower (in the order of 10^4 V/cm), the luminescent centers are excited via the recombination of electron-hole pairs and then relax to emit photons.

In recent years, oxide EL materials have shown application prospects in flat panel display technology because of their advantages in chemical stability against electron bombardment. Among the oxide materials, $ATiO_3$:Pr (A = Ca, Sr, Ba) has attracted considerable attention due to its application prospects in low-voltage field emission displays. $Ba_{1-x}Ca_xTiO_3$ is a ferroelectric

* Corresponding author. Guangdong Provincial Key Laboratory of Optical Information Materials and Technology & Institute of Electronic Paper Displays, South China Academy of Advanced Optoelectronics, South China Normal University, Guangzhou, 510006, China.
** Corresponding author.
E-mail addresses: 20198922@m.scnu.edu.cn (H. Sun), apkwkwok@polyu.edu.hk (K.W. Kwok).
Peer review under responsibility of The Chinese Ceramic Society.

https://doi.org/10.1016/j.jmat.2020.10.005

ceramic formed by replacing part of the Ba^{2+} in $BaTiO_3$ with Ca^{+}. Besides the typical ferroelectric and piezoelectric properties, the ceramics also exhibit a large electrostrictive strain that is strongly dependent on the content of Ca^{+}. C.N. Xu and Wang et al. have shown that, after doping with a small amount of Pr^{3+} (0.2 mol%), the ceramics (in the form of composite with an epoxy matrix) became multifunctional, exhibiting strong red mechanoluminescent and EL emissions [10]. Among the compositions, $Ba_{0.7}Ca_{0.3}TiO_3$:Pr contained both ferroelectric $Ba_{0.77}Ca_{0.23}TiO_3$:Pr grains and dielectric $Ba_{0.1}Ca_{0.9}TiO_3$:Pr grains, which also exhibited optimum luminescence properties. And the grains combined tightly together, with the latter grains sandwiched by and then interacted with the formers in three dimensions. Under an electric field, the ferroelectric grains provided surface charges and lattice dislocation on the grains. Because of the strong interaction, the luminescent centers in the dielectric grains were excited and then relaxed to the ground state by emitting photons.

Owing to the multifunctionality, piezoelectric/ferroelectric materials with rare-earth doping are promising for complex system applications in which the materials need to respond to electrical, mechanical and optical signals simultaneously [10,11]. Zhang et al. [12,13] have studied the EL mechanism of the $Ba_{1-x}Ca_xTiO_3$:Pr diphase ceramics and its relationship with mechanoluminescence based on a proposed dielectric/phosphor (ferroelectric)/dielectric sandwich structure. When the applied electric field was higher than the threshold electric field, electrons emitted from the interfaces were suggested to be driven into the phosphor layers by the Schottky emission and accelerated to become hot electrons for impacting and exciting Pr^{3+} to produce EL [12]. On the other hand, under an electric field below the threshold, the electrons combined with Pr^{3+}/h^{+} ionic complexes to form excited Pr^{3+}, which eventually relaxed to give rise to the EL [13]. The studies have also lighted the way to develop non-sulfide EL devices because of the dramatically simplification of the device fabrication process.

Most of the studies of non-sulfide oxide EL materials or devices focused on perovskite (Ba/Sr,Ca)TiO_3 or $CaTiO_3$ ceramics doped with Pr^{3+}. In general, only red EL emissions corresponding to the $^1D_2 \rightarrow {}^3H_4$ transition of Pr^{3+} were observed in composite samples comprising the ceramic powers [10,12,13] or in ceramic thin films [14]. In terms of other rare-earth elements doped perovskite oxide materials, green EL emission also has been studied around for years [15,16]. Unfortunately, research on blue EL emission technology in these systems has lagged behind. Blue EL emission is much more difficult, and it palys an important role in the progress of full-color inorganic electroluminescent display technology, which has been significantly troubling the scientific community and industry for decades [17,18]. Herein, this study is attempted to explore the possibilities of multicolor EL emission in perovskite piezoelectric materials. Inspired by its remarkable piezoelectric response, $Ba_{0.85}Ca_{0.15}Ti_{0.90}Zr_{0.10}O_3$ is chosen as the lead-free host in this work for providing a considerable piezoelectric potential under electric field [19]. Here, we report for the first time the observation of intense red EL emission in bulk $Ba_{0.85}Ca_{0.15}Ti_{0.90}Zr_{0.10}O_3$ piezoelectric ceramics doped by 0.2 mol% Pr^{3+} (abbreviated as BCTZ:Pr) and blue EL emission corresponding to the $^3P_1 \rightarrow {}^3H_4$ transition of Pr^{3+} in the composite counterpart comprising ceramic powers. The mechanisms have been investigated, with aim to extend our understanding of such a facile structure and non-sulfide EL device and thereby promoting their applications in lighting, display and wearable integrated device systems.

2. Material and methods

The BCTZ:Pr ceramics were prepared by solid-state reaction method. Two types of samples were prepared for EL characterization: ceramic disk and composite sheet. For the disk, the ceramic was thinned down to 250 μm and then coated with silver bottom electrode and transparent ITO top electrode. For the composite, the ceramic was first crushed and ground down to fine particles, then sieved and mixed with PDMS in a weight ratio of 7:3 to form a thin composite sheet (a thickness of 250 μm) on ITO-coated glass by spin-coating. The PDMS was a pre-mixed thoroughly with a curing agent in a weight ratio of 10:1. The sheet was then covered with another ITO-coated glass and cured at 70 °C for 2 h.

The crystallite structure was examined using XRD analysis (SmartLab, Rigaku Co., Japan). The morphology was studied using a SEM (JSM-6335F, JEOL Ltd., Japan). The dielectric properties were measured using an impedance analyzer (HP 4194A, Agilent Technologies Inc., Palo Alto, CA). The piezoelectric coefficient (d_{33}) was measured using a piezo-d_{33} m (ZJ-3A, China). A pre-poling procedure was taken before measuring the value of d_{33} and dielectric properties. A conventional Sawyer-Tower circuit was used to measure the polarization hysteresis (P-E) loop at 10 Hz. The photoluminescence excitation (PLE) and photoluminescence (PL) visible emission spectra were measured by a spectrophotometer (FLSP920, Edinburgh Instruments, UK). The EL spectra for the unpoled ceramic bulk and PDMS-based composite samples were recorded using an Ocean Optics USB4000 CCD spectrometer. A function generator (3390, Keithley, USA) together with a bipolar power amplifier (BOP 1000 M, Kepco, USA) were used to apply external voltage. A thermosluminescent meter (FJ427A1, Beijing Nuclear Instrument Factory, China) was used to measure the thermoluminescence (ThL) glow curve at a heating rate of 60 °C/min. The optical reflectance of the ceramics was measured in the range of 200–800 nm using a UV–vis–NIR spectrophotometer (UV-2550, Shimadzu Co., Japan) with an integrating sphere attachment (ISR-240A).

3. Results and discussions

The XRD pattern of the BCTZ:Pr ceramic in crushed powder form is shown in Fig. 1a. The phase parameters were determined by Rietveld refinement using the GSAS-EXPGUI program. And the $BaTiO_3$ coordinates in space group *R*3*m* and *P*4*mm* were selected as the fitting models. The full Rietveld analysis indicated the refined pattern well matched the experimental result, and the phase volume of BCTZ:Pr ceramic included 38.57% *R*3*m* and 61.43% *P*4*mm* with the fitting values of $\chi^2 = 1.892$, Rwp = 0.0519 and Rp = 0.0376. This suggested that the ceramic contains both the rhombohedral and tetragonal phases at room temperature and remains near the morphotropic phase boundary (MPB) after the doping of 0.2 mol% Pr, in consistence with the structure reported in our previous work [20]. Fig. 1b shows a typical example of a SEM micrograph of the cross section of the composite sample. The volume fraction of the BCTZ:Pr ceramic particles is about 45% and the sieved particles have a size of 20–50 μm by counting and statistics in the full range of SEM image. In agreement with the low tan δ observed at 1 kHz (2%), the ceramic particles and matrix are well connected, without forming too many pores that can markedly deteriorate the properties, in particular electrical properties. This evidently suggests that a high electric field can be applied to the sample and then to the ceramic particles without causing electrical breakdown for inducing the EL responses.

The temperature dependences of ε_r and tan δ for the BCTZ:Pr ceramic are shown in Fig. 1c. A strong dielectric peak arisen from the ferroelectric tetragonal-paraelectric cubic phase transition is observed at ~85 °C (T_C). As evidenced by the variation of tanδ, a very weak rhombohedral-tetragonal phase transition ($T_{R\text{-}T}$) is barely observed around 30 °C. This is in agreement with the XRD results

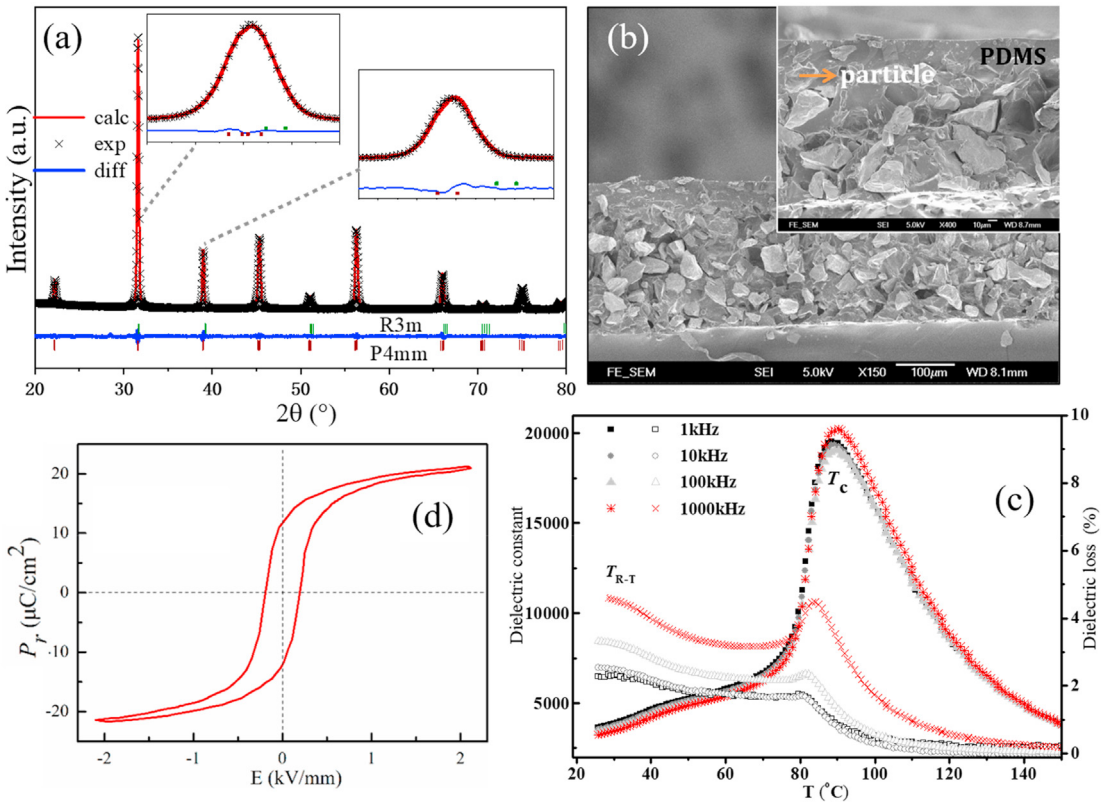

Fig. 1. XRD pattern and Rietveld refinement of the BCTZ:Pr ceramic(a); SEM micrograph of the cross section of the composite sample(b); temperature dependences of ε_r and tan δ for the BCTZ:Pr ceramic(c); P-E loop of ceramic (d).

that the ceramic contains both the rhombohedral and tetragonal phases at room temperature. As shown in Fig. 1d, the ceramic exhibits a typical P-E loop, revealing a large remanent polarization (P_r) of ~12 μC/cm^2 and a low coercive field (E_c) of ~0.21 kV/mm. The ceramic also exhibits good piezoelectric properties, such as a high piezoelectric charge coefficient (d_{33}) of ~410 pC/N and a large planar electromechanical coupling factor (k_p) of ~51%. It is known that there exists a softening effect in solid solutions near the MPB arisen from the presence of a greater number of possible spontaneous polarization directions, which makes domain rotation under electric field easier, and thus leading to a larger net polarization and then stronger piezoelectric response. The excellent piezoelectric properties are advantageous for inducing EL responses which will be discussed in the following section.

We examined the EL responses of the ceramic disk samples firstly. Under an ac electric (E) field of 10 kV/cm and 4 kHz, strong red light-emission is readily observed by naked eye from the BCTZ:Pr ceramic sample (schematic structure similar to our work [21]). A typical photograph of the light-emission is shown in Fig. 2a, while the EL spectra under E field of different amplitudes and frequencies are shown in Fig. 2b and c, respectively. In general, a broad emission band peaked at 613 nm is observed for the ceramic sample under various ac E fields. As illustrated in the insets, the peak EL intensity increases with increasing both the amplitude and frequency of the ac E field. A relatively low threshold E field (~4 kV/cm) is observed for the ceramic, above which the increase in the EL intensity becomes faster (Fig. 2b). Compared to other oxide EL ceramic, e.g., $Ba_{1-x}Ca_xTiO_3$:Pr ceramic, previous works reported the threshold E field even over 12 kV/cm [10,12]. The main reason for the threshold field distinction in different piezoelectric host should be related to the piezoelectric property, i.e., d_{33} value, and the low threshold field is an advantage of the ceramic in reducing energy consumption and assuring operational safety. Together with the simple device structure as compared to the conventional ones (having buffer and insulating layers), the BCTZ:Pr ceramic should become a promising material for EL applications. And it's expected that a large d_{33} value in piezoelectric materials may contribute to a decrease in threshold E field for the EL performance.

However, unlike the ceramic sample, the composite sample (comprising the BCTZ:Pr ceramic particles dispersed in a PDMS matrix) emits relatively weak blue light under an ac E field of 10 kV/cm and 2 kHz as illustrated in Fig. 3a. The emission bands at various ac E fields are broad, ranging from 400 nm to 600 nm (Fig. 3b and c). As shown in the inset of Fig. 3b, the peak EL intensity (at 473 nm) increases linearly with the amplitude of the E field, without showing any threshold in the same range of E field applied to the composite sample. This should be probably due to the effectively reduced pinning effect of ferroelectric domain walls since the ceramic particles were fine and sieved in the PDMS-based soft composites. Moreover, the emission band changes in shape as the E field frequency increases from 0.1 kHz to 4 kHz, showing a shift of the peak intensity to shorter wavelengths (from 544 nm to 473 nm). In the inset of Fig. 3c, the peak EL intensity reaches a maximum at 2 kHz. Similar results have been reported for EL ZnS:Cu phosphors by Ibañez et al. [22], in which the lifetime of the emitted photons is found to be proportional to their wavelength. As the frequency of applied E field increases, the predominance of photons with shorter wavelengths become higher, and thus yielding a shift of the EL intensity peak to shorter wavelengths. The effect is obviously more considerable for blue emission compared to red emission.

The PLE and PL spectra of the ceramic are shown in Fig. 4a for confirming the possible 4f4f and 4f5d transitions dof Pr^{3+} and the

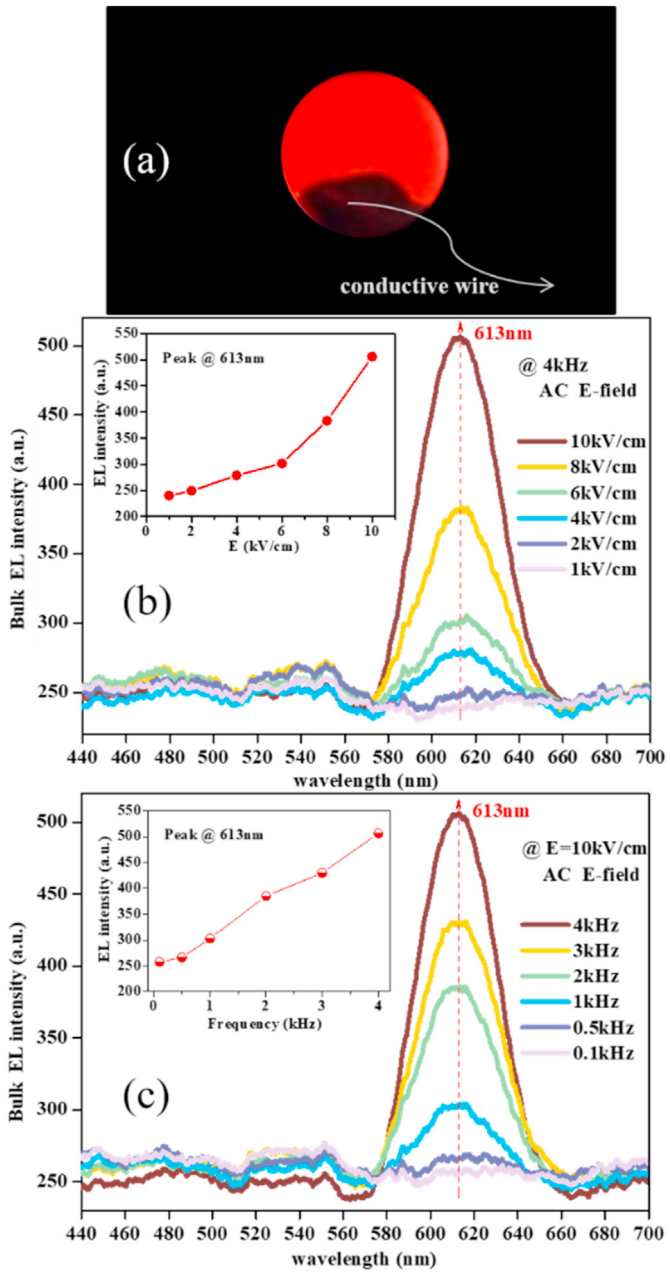

Fig. 2. EL responses of the ceramic disk sample: A typical photograph of the light-emission(a); EL spectra under E field of different amplitudes and frequencies (b) and (c), respectively.

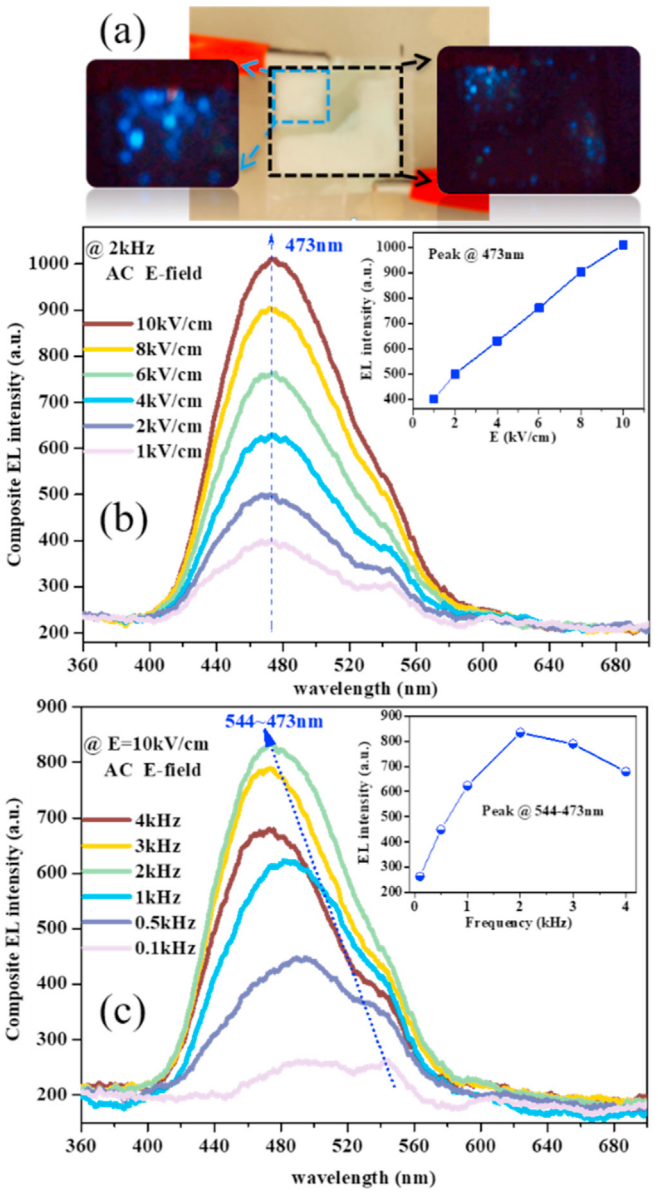

Fig. 3. EL responses of the composite sample: A typical photograph of the light-emission(a); EL spectra under E field of different amplitudes and frequencies (b) and (c), respectively.

relationship between the energy levels of Pr^{3+} and BCTZ. The broad PLE band in the range of 280–400 nm is resulted from the 4f to 4f5d transition of Pr^{3+}, valence-to-conduction band transition of the host, as well as the Pr-to-metal charge transfer state (CTS), as reported in the previous works [23–25]. As demonstrated by the spectra, electrons of Pr^{3+} can be excited to the 4f5d levels under UV irradiation, and then relax nonradiatively to the ^3P_J and $^1D_2$ levels for producing the greenish-blue ($^3P_J \rightarrow {}^3H_4$) and red ($^1D_2 \rightarrow {}^3H_4$) emissions, respectively. However, the ^3P_J emissions have been reported absent in certain PL materials, e.g., C–Y_2O_3:Pr^{3+} [26], and the overlap between the 4f5d levels of Pr^{3+} and the conduction band (CB) of the host has been suggested one of the causes for it. Owing to the overlap, the electron excited to the 4f5d levels will transfer to the CB and form a bound exciton state, [$Pr^{4+} + e_{CB}$], which will then relax nonradiatively via transferring its energy to excite electrons to the emitting $^1D_2$ level only. The quenching of the ^3P_J emissions can also be induced by the Pr-to-metal CTS, e.g., $Pr^{3+}/Ti^{4+} \rightleftarrows Pr^{4+}/Ti^{3+}$ in our system. Such a CTS forms a radiationless relaxation pathway for the excited electrons in the ^3P_J levels to the emitting $^1D_2$ level, and thus inducing partial or total quenching of the ^3P_J emissions. Based on these results, it can infer that the EL emission bands observed at ~613 nm for the ceramic sample (Fig. 2) and at ~473 nm for the composite sample (Fig. 3) are mainly attributed to the $^1D_2 \rightarrow {}^3H_4$ and $^3P_J \rightarrow {}^3H_4$ transitions of Pr^{3+}, respectively [23,27]. The quenching of the ^3P_J emissions is quite complete in the ceramic sample, which should be induced by the cross-relaxation through the 4f5d levels and CTS. It is known that a variety of defects will be formed during the high-temperature sintering in air atmosphere, which include Pr^{4+} and Ti^{3+} resulting from.

The oxidation of Pr^{3+} and reduction of Ti^{4+}, respectively. Together with the impurities in the raw materials, the CTS is reasonably expected to exist in the ceramic and composite samples. There also exist positively charged defects such as [$Pr_{Ba/Ca}$]^o and

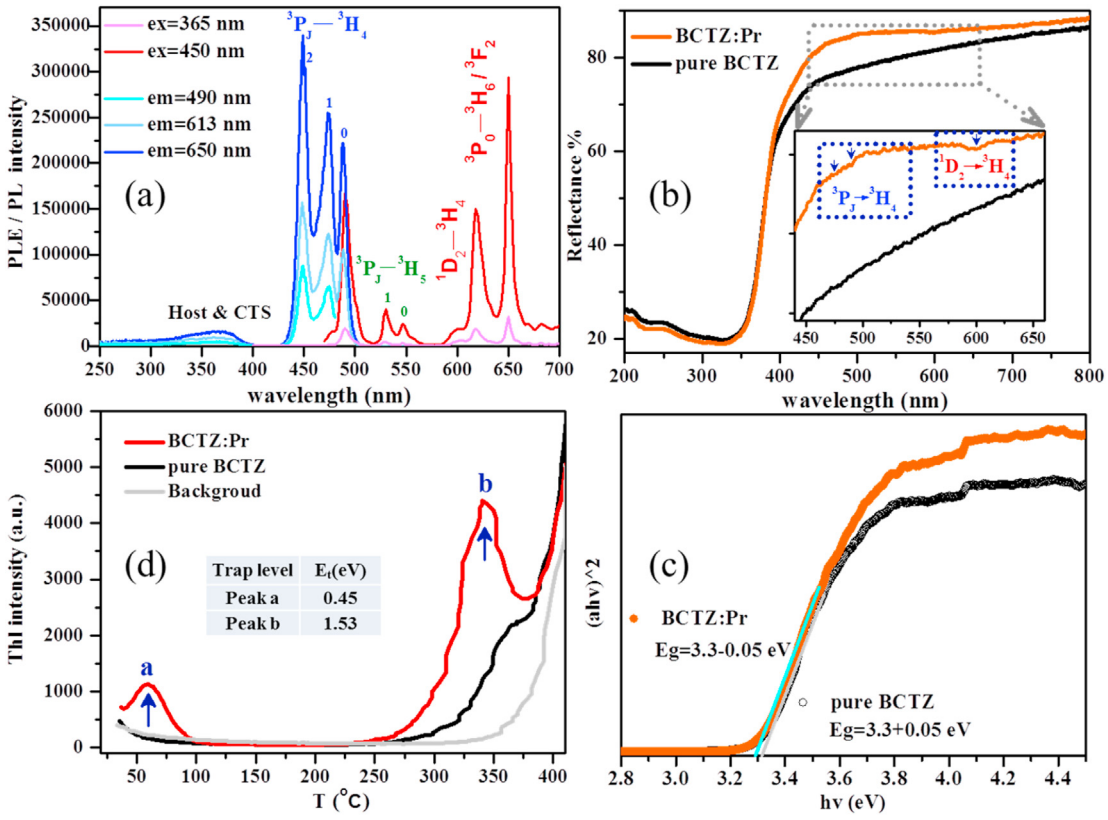

Fig. 4. PLE and PL spectra (a); UV–visible spectroscopy(b); corresponding Tauc plots(c), thermoluminescence measurements(d).

$[Pr_{Ba/Ca}]^{oo}$ arisen from the substitution of Pr^{3+} and Pr^{4+} in the A-site, respectively.

To further investigate the electron transitions, UV–visible spectroscopy using powder diffuse reflection method, band gap analysis and thermoluminescence (ThL) measurements were carried out for positioning the energy levels of Pr^{3+} and defects with respect to the valence and conduction band of host. As shown in Fig. 4b, in particular the inset showing the enlarged reflectance spectrum, typical absorptions arisen from the $^1D_2 \rightarrow {}^3H_4$ and $^3P_J \rightarrow {}^3H_4$ transitions of Pr^{3+} are observed in the BCTZ:Pr sample, but not in the BCTZ sample. Using the Kubelka-Munk function [28,29], the corresponding Tauc plots were calculated and the energy of the valence-to-conduction band transition of the host (from O^{2-} 2p levels to Ti/Zr 3d levels) is determined to be ~3.3 eV (375 nm), almost the same for both the BCTZ and BCTZ:Pr samples (Fig. 4c). As discussed, positively charged defects $[Pr_{Ba/Ca}]^{o}$ and $[Pr_{Ba/Ca}]^{oo}$ will be formed during the synthesis process, and which can serve as electron traps and then luminescent centers in luminescence processes. Obviously the trapped electrons will be released under thermal excitation [24,30,31]. The required energy or trap depth E_t can then be determined from the peak in a ThL glow curve, i.e. [32],

$$E_t = 2.52\left(\frac{kT_m{}^2}{\omega}\right) - 2kT_m$$

where T_m is the temperature at which the ThL intensity reaches a maximum, ω is the full width at half maximum of the ThL glow peak, and *k* is the Boltzmann constant. As shown in Fig. 4d, only the BCTZ:Pr sample exhibits two ThL glow peaks at 57 °C (330 K) and 340 °C (613 K), labelled as a and b, attributing to a shallow and deep electron trap, respectively. The corresponding trap depths are estimated to be 0.45 eV and 1.53 eV (below the CB). The former value (i.e., for the shallow trap) is similar to the value reported for Pr defects observed in Pr-doped $CaTiO_3$-based ceramics [30,31].

Based on the results, a schematic energy level diagram was established (Fig. 5) for elucidating the possible mechanisms of the observed EL emissions (Figs. 2 and 3). Although further X-ray photoelectron spectroscopy experiments are needed for the confirmation [30,33], the top of the valence band (VB) of the host is set as zero in Fig. 5 and the $^3H_4$ ground state of Pr^{3+} is located approximately at the top of the VB for illustration purposes. According to the energy level structure of Pr^{3+}, its $^3P_0$ state is located 2.6 eV above the $^3H_4$ ground state[12,26,30,34]. As evidenced by the broad PLE band in the range of 280–400 nm (Fig. 4a), the 4f5d levels are located within the CB of the host (before subject to an electric field). The shallow and deep electron traps are located based on the calculated trap depths E_t [32]. Clearly, the trapped electrons in shallow traps can easily be released under an external E field. For the ceramic sample (Fig. 5b), a large piezoelectric field is also induced by the external field across the sample because of the excellent piezoelectric properties ($d_{33} = 410$ pC/N). Then the released electrons are accelerated to become hot electrons for impacting and exciting Pr^{3+}. Because of the inevitable CTS discussed above and the overlap of the 4f5d levels with the CB, cross-relaxations occur and the excited electrons of Pr^{3+} are de-excited non-radiatively to the $^1D_2$ state to produce the red emissions (Fig. 2).

Unlike the ceramic sample, the BCTZ:Pr ceramic powders embedded in the soft PDMS matrix can easily be deformed by the (converse) piezoelectric effect, causing a bending of the CB [35]. That is, the converse piezoelectric strain effectively brings an elastic deformation in soft composite state, which induces piezo-charges as well as lattice dislocations at the grain interfaces, and then the internal electric fields make the local band structure (valence band and conduction band) bend slightly. Furthermore, there is a lot of papers reporting that the polarization charges/accumulated

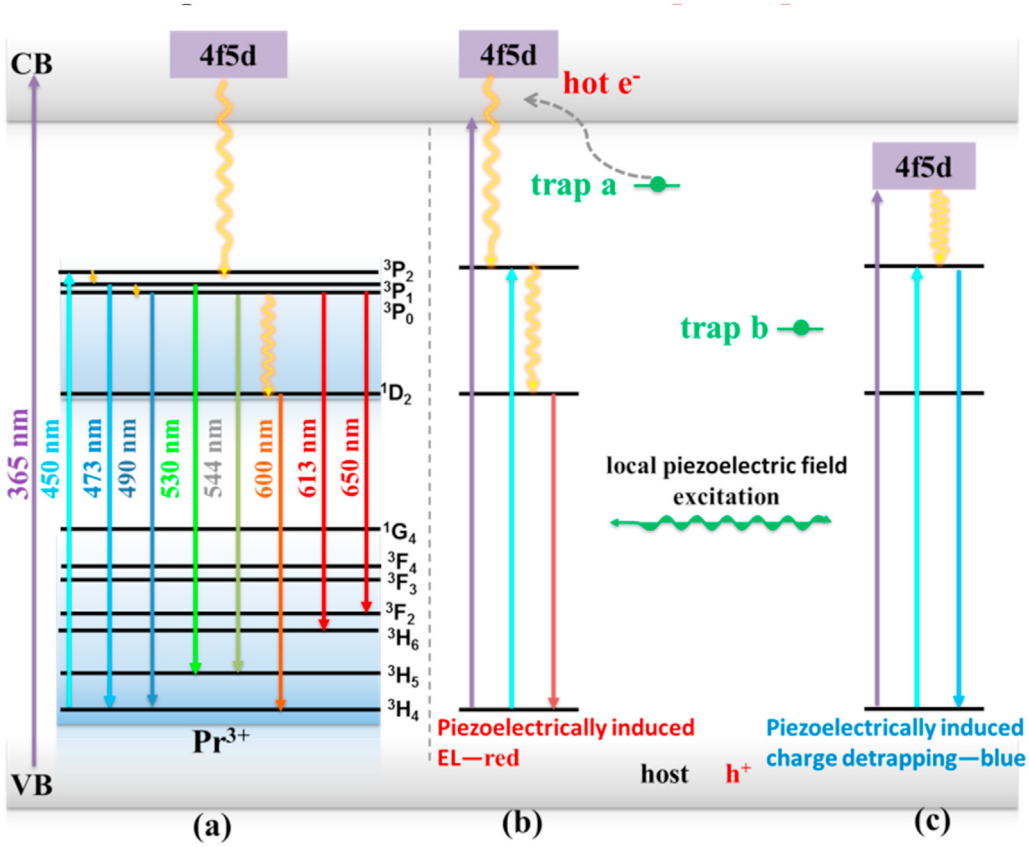

Fig. 5. Schematic energy level diagram: Initial state of host and Pr^{3+}(a); Mechanism of piezoelectrically induced-hot electrons mode and charge detrapping mode (b and c), respectively.

charges can bend the CB at the interfaces [36,37], which in turn induces a great change of the local crystal field around of Pr^{3+} [20,33,38]. Owing to the high sensitivity to the local crystal field, the 4f5d levels are considerably shifted below the CB (Fig. 5c). The electron traps are also shifted towards the CB, and the shallow ones may even fall within the CB. As a result, the charge carries in the deep traps can be released under the external E field and recombine subsequently with the Pr^{3+}/h^{+} ionic complexes to form excited Pr^{3+}. Owing to the larger amount of released energy, the electrons are excited to the 4f5d levels, which then relax nonradiatively to the ^3P_J levels for producing the blue emission (Fig. 3). As there is no overlap of the 4f5d levels and CB, the cross-relaxation through the Pr-to-metal CTS is hindered due to the lack of exciton states [$Pr^{4+}+e_{CB}$], which also facilitates the blue emission. Similar results have been reported for Pr-doped Y_2O_3 ceramic in which blue emissions are induced by an external high pressure via shifting the 4f5d levels below CB band [31,39]. Probably because of the few trapped charges, the observed blue emissions are weak. Nevertheless, the blue EL is obtained for the first time and it shows a great potential and value in further exploring inorganic blue color emitting and flexible ACEL devices.

4. Conclusions

In this paper, the EL responses of BCTZ:Pr (Pr^{3+}-doped $Ba_{0.85}Ca_{0.15}Ti_{0.90}Zr_{0.10}O_3$) lead-free ferroelectric ceramic and its PDMS-based composite have been investigated. The BCTZ:Pr ceramic emits a typical red emission (at 613 nm) under an AC E field, whereas a blue emission (at 473 nm) is observed in the composite sample. With reference to the PLE and PL spectra, the red and blue EL emissions are attributed to the $^1D_2 \rightarrow {}^3H_4$ and $^3P_J \rightarrow {}^3H_4$ transitions of Pr^{3+}, respectively. The electrons trapped in the shallow traps of the ceramic sample are released under an AC E field. In addition to the induced piezoelectric field, the de-trapped electrons are accelerated to become hot electrons for impacting and exciting Pr^{3+}. Owing to the cross-relaxations through the 4f5d levels and Pr-to-metal CTS, the ^3P_J emissions are completely quenched and thus only red emissions are observed. However, the external E field induces a large local piezoelectric deformation of the ceramic particles embedded in the PDMS matrix, which in turn causes a bending of the CB and then a downwards shift of the 4f5d levels from the CB. As a result, the cross-relaxations are hindered, and thus the blue EL emission is observed in the composite sample for further exploring inorganic full color ACEL devices.

Declaration of competing interest

The authors declare that they have no known competing financial interests or personal relationships that could have appeared to influence the work reported in this paper.

Acknowledgments

We appreciate this work was funded by Research Grant Council of Hong Kong Special Administrative Region (PolyU 152236/17E); Program for Chang Jiang Scholars and Innovative Research Teams in Universities (No. IRT_17R40), Science and Technology Program of Guangzhou (No. 201904020007), China Postdoctoral Science Foundation (2020M672667) and funded by Guangdong Provincial Key Laboratory of Optical Information Materials and Technology (2017B030301007).

References

[1] Larson C, Peele B, Li S, Robinson S, Totaro M, Beccai L, et al. Highly stretchable electroluminescent skin for optical signaling and tactile sensing. Science 2016;351(6277):1071–4.
[2] Wang L, Xiao L, Gu H, Sun H. Advances in alternating current electroluminescent devices. Adv Optical Mater 2019;7(7). 1801154.
[3] Yang CH, Chen B, Zhou J, Chen YM, Suo Z. Electroluminescence of giant stretchability. Adv Mater 2016;28(22):4480–4.
[4] Wang J, Yan C, Cai G, Cui M, Eh AL-S, Lee PS. Extremely stretchable electroluminescent devices with ionic conductors. Adv Mater 2015;28(22):4490–6.
[5] Yamauchi Y, Takeda M, Kakihara Y, Yoshida M, Kawaguchi J, Kishishita H, et al. Inherent memory effects in ZnS: Mn thin film EL devices. International Electron Devices Meeting (IEDM). IEEE 1974:348–51.
[6] Barrow WA, Coovert RE, King CN. Tech. Digest SIDvol. 84. Society for Information Display; 1984. p. 249.
[7] Erkki S, Marja L. Method for preparing a multilayer structure for electroluminescent components, us patent. 1996. 5496597.
[8] Stauffer F, Tybrandt K. Bright stretchable alternating current electroluminescent displays based on high permittivity composites. Adv Mater;28(33): 7200–7203.
[9] Robert W, Jack S, Paul H, Ireland TG, Marsh PJ. AC powder electroluminescent displays. Journal of the SID 2011;19/11:798.
[10] Wang X, Xu CN, Yamada H, Nishikubo K, Zheng X-G. Electro-mechano-optical conversions in Pr^{3+}-doped $BaTiO_3$-$CaTiO_3$ ceramics. Adv Mater 2005;17(10): 1254–8.
[11] Wang Y, Luo C, Wang S, Chen C, Yuan G, Luo H, et al. Large piezoelectricity in ternary lead-free single crystals. Adv Electronic Mater 2020;6(1). 1900949.
[12] Zhang JC, Wang X, Yao X, Xu C-N, Yamada H. Studies on AC electroluminescence device made of $BaTiO_3$-$CaTiO_3$: Pr^{3+} diphase ceramics. Appl phys express 2010;3(2). 022601.
[13] Zhang JC, Wang X, Yao X, Xu C-N, Yamada H. Strong elastico-mechanoluminescence in diphase $(Ba,Ca)TiO_3$:Pr^{3+} with Self-assembled sandwich architectures. J Electrochem Soc 2010;157(12):G269.
[14] Kyömen T, Aramaki K, Kakubari Y, Takashima H. Effects of doping by aluminum or lanthanum on the electrical and electroluminescence properties of $Ca_{0.6}Sr_{0.4}TiO_3$:Pr thin films. J Lumin 2019;207:424–9.
[15] Sun JM, Skorupa W, Dekorsy T, Helm M, Rebohle L, Gebel T. Bright green electroluminescence from Tb^{3+} in silicon metal-oxide-semiconductor devices. J Appl Phys 2005;97(12). R1169.
[16] Guangmiao W, Shenwei W, Miaoling H, Yanwei Z, Kai O, Li Y. Green electroluminescence from Tb_2O_3/polymer heterojunction light-emitting diodes. J Mater Sci 2018;53:13949–54.
[17] Lin K, Xing J, Quan LN, Pelayo F, Gong X, Lu J, et al. Perovskite light-emitting diodes with external quantum efficiency exceeding 20 per cent. Nature 2018;562:245–8.
[18] Liu Y, Cui J, Du K, Tian H, He Z, Zhou Q, et al. Efficient blue light-emitting diodes based on quantum-confined bromide perovskite nanostructures. Nat Photon 2019;13:760–4.
[19] Koruza J, Bell AJ, Frömling T, Webber KG, Wang K, Rödel J. Requirements for the transfer of lead-free piezoceramics into application. J Materiomics 2018;4: 13–26.
[20] Sun H, Wu X, Chung TH, Kwok KW. In-situ electric field-induced modulation of photoluminescence in Pr-doped $Ba_{0.85}Ca_{0.15}Ti_{0.90}Zr_{0.10}O_3$ lead-free ceramics. Sci Rep 2016;6:28677.
[21] Sun H, Wu X, Peng DF, Kwok KW. Room-temperature large and reversible modulation of photoluminescence by in situ electric field in ergodic relaxor ferroelectrics. ACS Appl Mater Interfaces 2017;9(39):34042–9.
[22] Ibañez J, Garcia E, Gil L, Mollar M, MaríB. Frequency-dependent light emission and extinction of electroluminescent ZnS:Cu phosphor. Displays 2007;28(3):112–7.
[23] Jia W, Jia D, Rodriguez T, Evans DR, Meltzer RS, Yen WM. UV excitation and trapping centers in $CaTiO_3$:Pr^{3+}. J Lumin 2006;119–120:13–8.
[24] Zhang JC, Wang X, Yao X. Enhancement of luminescence and afterglow in $CaTiO_3$:Pr^{3+} by Zr substitution for Ti. J Alloys Compd 2010;498(2):156.
[25] Rétot H, Bessière A, Viana B, LaCourse B, Mattmann E. 5d-4f and 4f-4f emissions in Ln-doped sesquioxide ceramics. Opt Mater 2011;33(7):1008–11.
[26] Srivastava AM, Renero LC, Santamaría P, Rodríguez F, Valiente R. Pressure-induced Pr^{3+} P_0 luminescence in cubic Y_2O_3. J Lumin 2014;46:27–32.
[27] Boutinaud P, Pinel E, Dubois M, Vink AP, Mahiou R. UV-to-red relaxation pathways in $CaTiO_3$:Pr^{3+}. J Lumin 2005;11(1–2):69–80.
[28] Mahata MK, Koppe T, Mondal T, Brüsewitz C, Kumar K, Rai VK, et al. Incorporation of Zn^{2+} ions into $BaTiO_3$:Er^{3+}/Yb^{3+} nanophosphor: an effective way to enhance upconversion, defect luminescence and temperature sensing. Phys Chem Chem Phys 2015;17(32). 20741.
[29] Lin J, Zhou Y, Lu Q, Wu X, Lin C, Lin T, et al. Reversible modulation of photoenergy in Sm-doped $(K_{0.5}Na_{0.5})NbO_3$ transparent ceramics via photochromic behavior. J Mater Chem 2019;7:19374–84.
[30] Zhang JC, Long YZ, Wang X, Xu C-N. Controlling elastic-mechanoluminescence in diphase $(Ba,Ca)TiO_3$:Pr^{3+} by co–doping different rare earth ions. RSC Adv 2014;4(77):40665–75.
[31] Zhang JC, Long YZ, Yan X, Wang X, Wang F. Creating recoverable mechanoluminescence in piezoelectric calcium niobates through Pr^{3+} doping. Chem Mater 2016;8(11):4052–7.
[32] Zhang S, Hu Y, Chen L, Ju G, Wang T, Wang Z. Luminescence properties of the pink emitting persistent phosphor Pr^{3+}-doped $La_3GaGe_5O_{16}$. RSC Adv 2015;5(47):37172–9.
[33] Zhang Z-J, Ten Kate OM, Delsing, Kolk EV, Notten PHL, Dorenbos P, et al. Photoluminescence properties and energy level locations of RE^{3+} (RE = Pr, Sm, Tb, Tb/Ce) in $CaAlSiN_3$ phosphors. J Mater Chem 2012;22(19):9813.
[34] Dieke GH. Spectra and energy levels of rare earth ions in crystals. New York: Interscience Publications; 1968.
[35] Ratnesh T, Vikas D, Chandra BP. Exact model for the elastico mechanoluminescence of ii–vi phosphors. Mater Phys Mech 2014;19:25–38.
[36] Wang X, Peng D, Huang B, Pan C, Wang ZL. Piezophotonic effect based on mechanoluminescent materials for advanced flexible optoelectronic applications. Nanomater Energy 2018;55:389–400.
[37] Morozovska AN, Eliseev EA, Svechnikov SV, Krutov AD, Shur VY, Borisevich AY, et al. Finite size and intrinsic field effect on the polar-active properties of the ferroelectric-semiconductor heterostructures. Phys Rev B 2010;81(20):2498–502.
[38] Zheng M, Sun H, Chan MK, Kwok KW. Reversible and nonvolatile tuning of photoluminescence response by electric field for reconfigurable luminescent memory devices. Nanomater Energy 2019;55:22–8.
[39] Shen Y, Gatch DB, Rodríguez Mendoza UR, Cunningham G, Meltzer RS, Yen WM, et al. Ce^{3+} luminescence in C–Lu_2O_3. Phys Rev B 2002;65. 212103.

Hailing Sun obtained BSc and MSc in 2011 and 2014 from Sichuan Normal University, and then received PhD in 2018 from Department of Applied Physics, Hong Kong Polytechnic University under the supervision of Prof. K.W. Kwok. Now she is working at South China Normal University. Her research interests include the coupling between smart piezoelectric materials and tunable luminescence for multi-functional applications, and ambient mechanical energy harvesting.

Manchung Wong received his MSc in 2016 and PhD degrees in 2019 from the Department of Applied Physics, Hong Kong Polytechnic University. He is now working as research fellow at Hong Kong Polytechnic University. His research is related to smart and functional piezoelectric material, ambient mechanical energy harvesting and actuation, and triboelectric generator.

Guofu Zhou completed his dual PhD in materials science at Chinese Academy of Sciences in 1991, and in Physics at University of Amsterdam in 1994, respectively. He is now working as full professor of South China Normal University and the dean of the South China Academy of Advanced Optoelectronics. His research is related to the field of micro/nano optoelectronic materials, devices and flat panel displays, mainly engaged in research on optoelectronic materials and devices.

K.W. Kwok received his Ph.D. degree from The Hong Kong Polytechnic University in 1997. Currently, he takes up a full professorship and associate deanship at Faculty of Applied Science and Textiles in The Hong Kong Polytechnic University. His research focuses on processing, characterization and applications of ferroelectric materials, electro-optic materials, and photoluminescence materials.